Molecular Therapy
Nucleic Acids
Original Article

Inhibition of IKKβ/NF-κB signaling facilitates tendinopathy healing by rejuvenating inflamm-aging induced tendon-derived stem/progenitor cell senescence

Chongyang Wang,[1,4] Zhekun Zhou,[1,4] Wei Song,[1] Zhuochang Cai,[1] Zhenyu Ding,[1] Daoyun Chen,[1] Fangfang Xia,[3] and Yaohua He[2]

[1]Department of Orthopaedics, Shanghai Jiao Tong University Affiliated Sixth People's Hospital, 600 Yishan Road, Shanghai 200233, China; [2]Department of Orthopaedics, Jinshan Branch of Shanghai Sixth People's Hospital affiliated to Shanghai University of Medicine & Health Sciences, 147 Jiankang Road, Shanghai 201503, China; [3]Department of Instrument Science and Engineering, School of Electronic Information and Electrical Engineering, Shanghai Jiao Tong University, 800 Dongchuan Road, Shanghai 200240, China

Degenerative rotator cuff tendinopathy (RCT) is a chronic tendon disease caused by degeneration and inflammation, which often affects the elderly population. Mesenchymal stem cell senescence is generally recognized as an important pathophysiological mechanism in many age-related skeletal diseases. Herein, we collected human tendon-derived stem/progenitor cells (TSPCs) from degenerative supraspinatus tendons and found that TSPC senescence is closely related to RCT. We further identified that nuclear factor κB (NF-κB) pathway activation is involved in age-related inflammation (inflamm-aging) of degenerative RCT. Moreover, whole genome RNA sequencing revealed that *in vitro* inhibition of the I kappa B kinase β (IKKβ)/NF-κB signaling pathway could reverse the aged TSPC phenotype with decreased TSPC senescence and increased tenogenic potential. To achieve effective *in vivo* inhibition of IKKβ/NF-κB signaling, we fabricated IKKβ small interfering RNA (siRNA)-loaded gold nanoclusters (AuNC-siRNA) for efficient and convenient intra-articular delivery of IKKβ siRNA. We found that AuNC-siRNA prevented inflamm-aging-induced TSPC senescence and dysfunction in a degenerative RCT aged rat model. Together, these data show that inflamm-aging causes degenerative RCT through inducing TSPC senescence, which can be reversed by blocking the IKKβ/NF-κB pathway *in vivo*. Thus, our study provides a promising therapeutic strategy for degenerative RCT via intra-articular delivery of IKKβ siRNA using AuNCs.

INTRODUCTION

Shoulder pain owing to degenerative rotator cuff tendinopathy (RCT) is the third most common musculoskeletal complaint.[1,2] As degenerative RCT progresses, it may lead to a partial or complete tear of the tendon, which generally requires reparative surgery. Each year, approximately 250,000 patients undergo rotator cuff repair surgery in the United States[3]; however, the surgical repair failure rate is almost 40% owing to the degenerative pathologies of the patients' rotator cuff tendons.[4] Hence, understanding the cellular and molecular mechanisms underlying degenerative RCT is vital for clinicians to design novel therapeutics to prevent the occurrence of tendon tears as well as improve surgical outcomes.

Degenerative RCT is commonly recognized as an age-dependent, intrinsic, degenerative disease.[5] Mesenchymal stem cell (MSC) senescence is an important pathophysiological mechanism related to many degenerative skeletal disorders.[6,7] Age-related inflammation (inflamm-aging) is characterized by sterile, chronic, low-grade inflammation that contributes to the aging process and to the pathogenesis of age-related diseases.[8,9] It is deemed to be a major contributor to MSC senescence.[10] However, the impact of inflamm-aging on tendon-derived stem/progenitor cell (TSPC) senescence in degenerative RCT is still unclear. To fill this knowledge gap, we hypothesized that inflamm-aging induces TSPC senescence, which thereby contributes to degenerative RCT development in the elderly population. Recently, Josephson et al.[11] reported that nuclear factor κB (NF-κB) signaling is closely related to inflamm-aging-triggered skeletal stem/progenitor cell dysfunction and impaired bone

Received 2 November 2021; accepted 15 December 2021;
https://doi.org/10.1016/j.omtn.2021.12.026.

[4]These authors contributed equally

Correspondence: Yaohua He, Department of Orthopaedics, Jinshan Branch of Shanghai Sixth People's Hospital affiliated to Shanghai University of Medicine & Health Sciences, 147 Jiankang Road, Shanghai 201503, China
E-mail: heyaohua@sjtu.edu.cn
Correspondence: Fangfang Xia, Department of Instrument Science and Engineering, School of Electronic Information and Electrical Engineering, Shanghai Jiao Tong University, 800 Dongchuan Road, Shanghai 200240, China.
E-mail: xiafang09@126.com
Correspondence: Daoyun Chen, Department of Orthopaedics, Shanghai Jiao Tong University Affiliated Sixth People's Hospital, 600 Yishan Road, Shanghai 200233, China.
E-mail: dychen1218@163.com

healing in aged mice. Meanwhile, Abraham et al.[12] observed an increase in NF-κB signaling in chronic overuse-induced RCT. They found that genetic conditional knockout of I kappa B kinase β (IKKβ) in tendon fibroblasts can alleviate chronic overuse-induced tendinopathy.[12] Despite this, the efficacy of *in vivo* IKKβ/NF-κB signaling inhibition on reversing inflamm-aging-induced TSPC senescence and treating degenerative RCT is still unclear and requires further study.

In this study, we first separated TSPCs from healthy human hamstring tendons and degenerative supraspinatus tendons to explore the association between TSPC senescence and degenerative RCT. Then, we assayed the NF-κB pathway to determine its potential role in inflamm-aging-induced TSPC senescence. Thereafter, we used a one-step reaction to fabricate IKKβ siRNA-loaded gold nanoclusters (AuNC-siRNA) for efficient and convenient intra-articular administration, leading to IKKβ/NF-κB pathway blocking, with the aim of improving the function of senescent TSPCs. Our results indicated that the inhibition of IKKβ/NF-κB signaling prevents the development of degenerative RCT through stimulating improved TSPC senescence, which provides a novel potential target and approach for treating inflamm-aging-induced degenerative RCT.

RESULTS

Senescent TSPCs accumulate in human degenerative rotator cuff tendons

We first compared the difference between TSPCs isolated from healthy hamstring tendons (H-TSPCs) and degenerative supraspinatus tendons (S-TSPCs). Pronounced morphological differences were noticed between H-TSPCs and S-TSPCs. For example, the H-TSPCs were spindle- or cobble-stone-shaped, while the S-TSPCs were round and flattened (Figures 1A, 1B, and S1). Through flow cytometric analysis, we found no difference in the expression of stem cell-related surface markers on the S-TSPCs and H-TSPCs (Figure S2). Regarding tri-lineage differentiation, S-TSPCs showed reduced osteogenic and chondrogenic differentiation potential, as well as increased adipogenic differentiation potential when compared with those of H-TSPCs (Figures 1C and 1D).

Cellular senescence assay showed that the proportion of senescence-associated β-galactosidase (SA-β-gal)-positive S-TSPCs was markedly higher than that of SA-β-gal-positive H-TSPCs (Figure 1E). Moreover, immunofluorescence staining of aging markers showed significantly higher $p16^{INK4A}$ and $p21^{CIP1}$ expression in S-TSPCs than in H-TSPCs (Figures 1F and 1G). Quantitative reverse transcription-polymerase chain reaction (qRT-PCR) analysis also showed that the expression of senescence-associated secretory phenotype (SASP)-related genes (*IL6*, *IL1A*, *CXCL1*, *CXCL2*, and *CDKN2A* (*P16*)) was upregulated in S-TSPCs (Figure 1H). In addition, Picrosirius red staining and tenogenesis-related gene analysis (*SCX*, *BGN*, *TNMD*, *DCN*, *COL1*, and *COL3*) showed that the tenogenic differentiation capacity of S-TSPCs was inferior to that of H-TSPCs (Figures 1I and 1J), which accounts for the impaired tendon regeneration potential in aged patients.

NF-κB signaling pathway is activated in senescent TSPCs

Nuclear localization is a prerequisite for NF-κB p65 phosphorylation, which activates the NF-κB pathway. To clarify the role of NF-κB signaling in TSPC senescence, we assayed NF-κB signaling activation using Western blotting for phosphorylated NF-κB p65 (NF-κBp-p65). The Western blotting results showed that the p-p65/p65 level in S-TSPCs was significantly higher than that of H-TSPCs (Figures 2A and 2B). We also found that the nuclear NF-κB p65 localization in S-TSPCs was increased three-fold compared with that in H-TSPCs (Figures 2C and 2D). These data demonstrate that the NF-κB signaling pathway is activated during TSPC senescence.

In vitro blocking of NF-κB mitigates TSPC senescence

To screen IKKβ siRNA sequences for the most effective IKKβ/NF-κB pathway inhibition, four different IKKβ siRNAs were designed and transfected to TSPCs. The qRT-PCR and Western blotting assay demonstrated that IKKβ siRNA sequence 2 could achieve the most effective knockdown of IKKβ (Figure S3). Thus, it was used for subsequent experiments.

Pre-transfection with IKKβ siRNA suppressed IL-1β-induced NF-κB signaling activation (Figures 2E–2H), which subsequently mitigated TSPC senescence with decreased percentage of SA-β-gal-positive cells (Figures 2I and 2J) and $p16^{INK4a}$- and $p21^{CIP1}$-positive TSPCs (Figures 2K and 2L).

The whole messenger RNA (mRNA) expression in IL-1β-treated TSPCs with or without IKKβ knockdown was detected using RNA sequencing. Hierarchical clustering analysis showed a stark separation between IL-1β-treated and IL-1β + IKKβ siRNA-treated TSPCs (Figure 3A). Kyoto Encyclopedia of Genes and Genomes (KEGG) pathway analysis demonstrated that IKKβ blocking downregulated signaling pathways in cellular senescence and proinflammatory phenotypes (Figure 3B). In addition, a gene set enrichment analysis further revealed that IKKβ blocking increased the expression of genes associated with stemness and proliferation, while it also decreased the expression of genes associated with cellular aging and adipogenic potential (Figure 3C). Taken together, these data reveal that IKKβ silencing decreases TSPC senescence.

AuNCs efficiently load and deliver IKKβ siRNA

Core AuNC has a diameter of 2.6 ± 0.2 nm (Figures 4A and 4B). After IKKβ siRNA binding, the diameter of the AuNC-siRNA increased to 100 ± 10.6 nm (Figures 4C and 4D). Owing to the amine-derived positive charge of glutathione (GSH) and oligoarginine, the surface charge of the AuNCs was 18.47 ± 0.59 mV. After absorbing the anionic siRNA, the surface charge of AuNC-siRNA decreased to 16.90 ± 0.72 mV (Figure 4E). To further confirm siRNA adsorption into the AuNCs, the changes in atomic composition were monitored using X-ray photoelectron spectra (XPS) analysis. After siRNA binding, the surface Au and S content of AuNC-siRNA decreased, while C, N and O content slightly increased. Owing to the presence of phosphates and nucleotides in the siRNA molecules, the surface P content

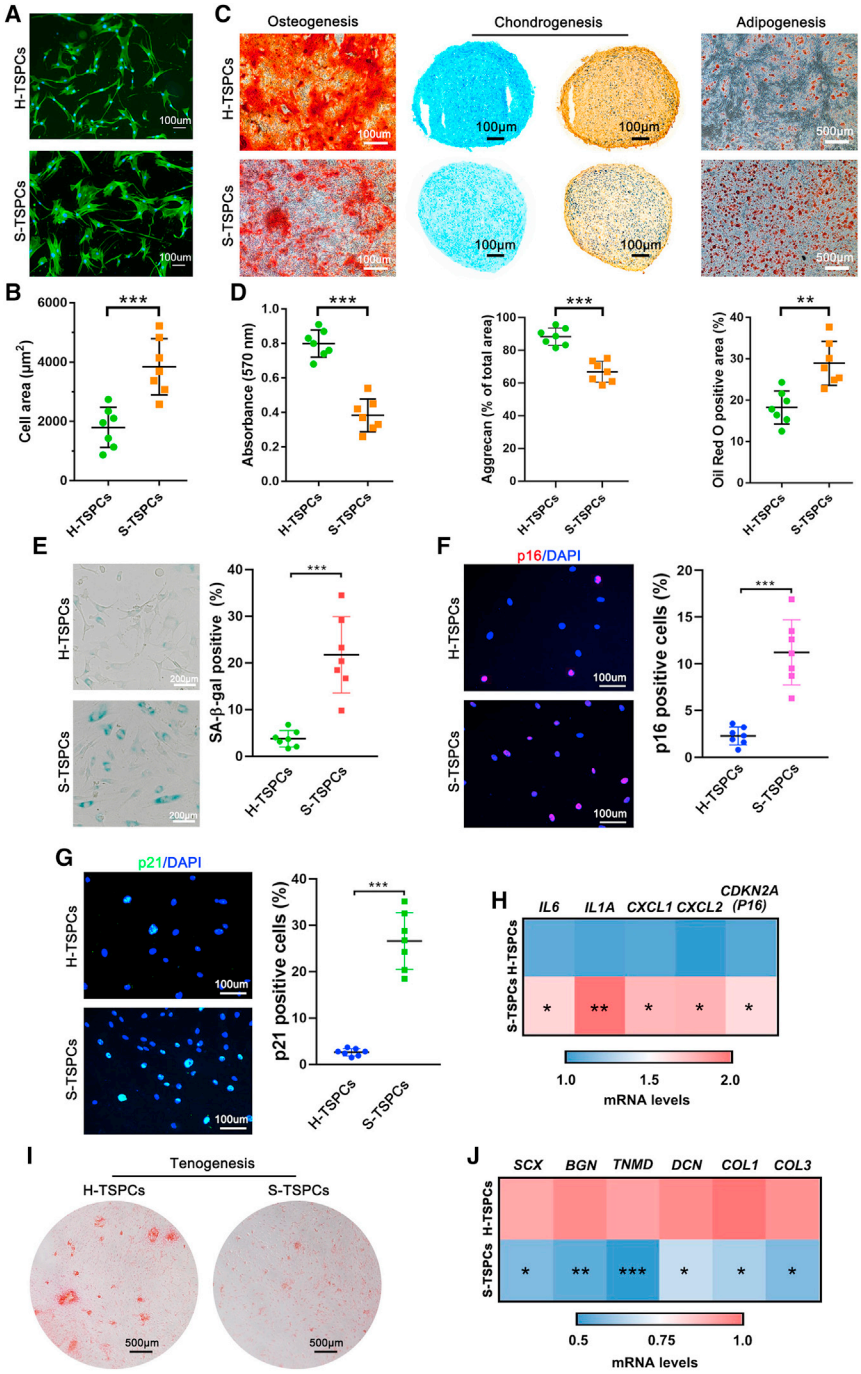

Figure 1. Histological staining reveals senescent TSPCs accumulate in human degenerative supraspinatus tendons

(A) Phalloidin-stained green actin fibers of H-TSPCs and S-TSPCs. (B) Quantification of cell area (n = 7 per group). Two hundred cells in each donor group were analyzed. (C) Alizarin Red S, Alcian blue, type II collagen, and Oil Red O staining for osteogenesis, chondrogenesis, and adipogenesis analysis of H-TSPCs and S-TSPCs. (D) Quantification of Alizarin Red S, Alcian blue and Oil Red O staining (n = 7 per group). (E) SA-β-gal staining and quantification of senescent cells in H-TSPCs and S-TSPCs (n = 7 per group). (F) Immunofluorescence staining (red) and quantification of $p16^{INK4A}$ positive cells (n = 7 per group). (G) Immunofluorescence staining (green) and quantification of $p21^{CIP1}$ positive cells (n = 7 per group). (H) qRT-PCR analysis of SASP-related gene expression in H-TSPCs and S-TSPCs (n = 7 per group). (I) Sirius red staining for evaluating tenogenic differentiation ability of H-TSPCs and S-TSPCs (n = 7 per group). (J) qRT-PCR analysis of tenogenesis-related gene expression in H-TSPCs and S-TSPCs (n = 7 per group). H-TSPCs, TSPCs isolated from healthy hamstring tendons. S-TSPCs, TSPCs isolated from degenerative supraspinatus tendons. *p < 0.05, **p < 0.01, ***p < 0.001.

of AuNC-siRNA was substantial (Figure 4F). Hence, these data demonstrated the successful adsorption of siRNA into AuNCs.

The live/dead staining assay (Figures 4G and 4H), CCK-8 assay (Figure 4I), and flow cytometry analysis (Figure 4J) showed no significant influence of 1–100 ng/mL AuNCs on cell proliferation, viability, or cell cycle. Thus, these results confirmed the *in vitro* biocompatibility of AuNCs with TSPCs.

Next, an electrophoretic mobility shift assay was performed to evaluate the effect of AuNCs on siRNA stability by antagonizing RNase degradation. After incubating with various RNase concentrations, the free siRNA was completely degraded, and no free siRNA was detected on the gel (Figure 5A). After adsorbing into the AuNCs, AuNC-siRNA consistently resisted siRNA degradation by RNase (Figure 5B). During the cellular uptake assay, almost no free siRNA could enter the TSPCs owing to its negative charge and high molecular weight. In contrast, AuNC-siRNA successfully entered into TSPCs (Figure 5C). This demonstrated that the AuNC-siRNA complex can elevate siRNA internalization efficiency. The IKKβ gene knockdown efficiency of the AuNC-siRNA complex was 76.9%, which was significantly greater than that of free siRNA (8.8%) and AuNC-nonsense siRNA (AuNC-nsRNA, 6.4%) (Figure 5D). The efficiency of AuNC-siRNA showed no significant difference from that of RNAiMAX-transfected siRNA (RNAiMAX-siRNA) in inhibiting IKKβ mRNA expression (78.6%). Levels of IKKβ protein was consistently the lowest in AuNC-siRNA-treated TSPCs (Figures 5E and 5F).

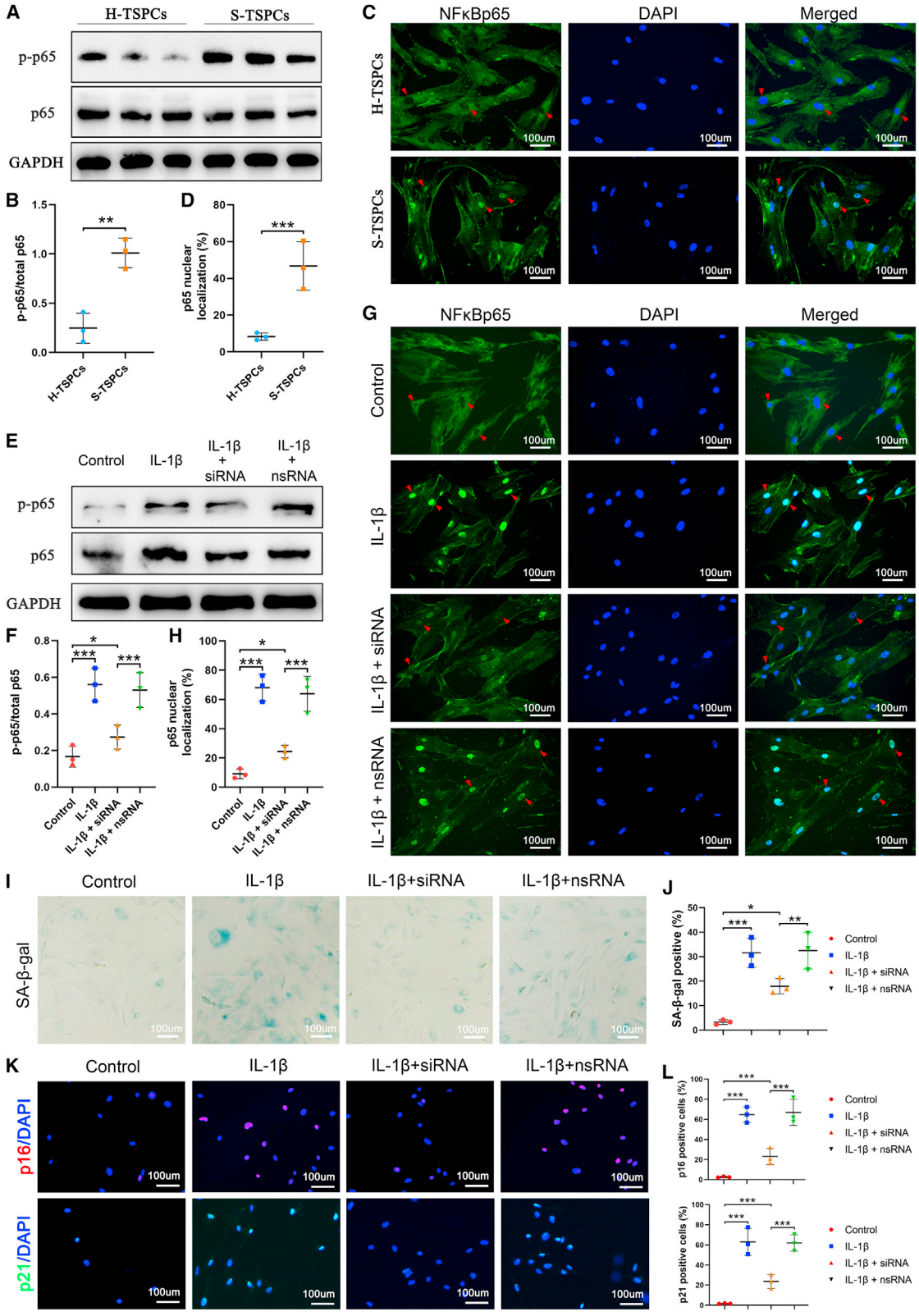

(legend on next page)

In vivo blocking of NF-κB activation by AuNC-siRNA attenuates inflamm-aging-triggered rat RCT

Hematoxylin and eosin (H&E)-stained supraspinatus tendons in young rats seemed to be fine, organized, straight, and polar collagen bundles. In contrast, the collagen fiber alignment was disrupted and altered in the old rats, which is consistent with the histological characterization of degenerative tendons in humans.[13] The cellularity increased around the tendon-to-bone insertion site in the old rats. Subacromial AuNC-siRNA injection improved collagen fiber orientation; however, free siRNA and AuNC-nsRNA administration did not improve the altered collagen fiber structure (Figure 6A). As the major structural and mechanical component of tendon tissue, type I collagen was stained and quantified. Type I collagen staining intensity was significantly decreased in the old group. Intra-articular administration of AuNC-siRNA prevented the loss of type I collagen (Figures 6B and 6C). Contrary to this, levels of type III collagen were increased in the old group and decreased by AuNC-siRNA administration (Figures 6D and 6E). According to a previous study, an increase in type III collagen levels generally occurs as a repair response to tendon degeneration. This may inhibit the regeneration of collagen fibrils and lead to tendons that are less resistant to stress and prone to rupture.[14] Therefore, our results suggest that AuNC-siRNA exerted a positive influence on the regeneration of tendon tissue as opposed to the development of scar tissue in degenerative rotator cuff tendons. Consistent with the results of histological analysis, biomechanical testing revealed that the maximum load, stress, and modulus decreased in old rats. After AuNC-siRNA treatment for 3 months, the biomechanical properties of tendons were significantly improved (Figures 6F and 6G).

AuNC-siRNA attenuates degenerative RCT by inhibiting TSPC senescence

To further explore whether the therapeutic effects of AuNC-siRNA on degenerative RCT include the inhibition of TSPC senescence, rat TSPCs were isolated and analyzed *ex vivo*. First, NF-κB activation was analyzed using p65 immunofluorescence. Consistent with that in TSPCs from human degenerative RCT tendons, the NF-κB pathway was activated and inhibited by AuNC-siRNA in TSPCs from the supraspinatus tendons of old rats. However, the free siRNA and AuNC-nsRNA failed to decrease *in vivo* NF-κB pathway activation (Figures 7A and 7B). Then, we found that the percentage of SA-β-gal-positive TSPCs significantly increased in old rats, which was subsequently significantly mitigated by AuNC-siRNA administration (Figures 7C and 7D). Immunofluorescence staining of aging markers showed $p21^{CIP1}$ and γH2AX-stained TSPCs were less abundant in the AuNC-siRNA group than that in the old, free siRNA, and AuNC-nsRNA groups (Figures 7E–7H).

Moreover, Picrosirius red staining and tenogenesis-related gene expression (*Scx*, *Tnmd*, and *Col1*) in TSPCs showed the improved tenogenic potential of TSPCs isolated from AuNC-siRNA-treated rats (Figures 7I and 7J). Thus, we conclude that AuNC-siRNA alleviates inflamm-aging-triggered degenerative RCT by inhibiting TSPC senescence (Figure 8). Alongside this, the H&E-stained organ tissues (liver, lung, kidney, heart, and spleen) were used to assay *in vivo* AuNC toxicity. No noticeable inflammation or injury was observed, further demonstrating its *in vivo* biocompatibility (Figure S4).

DISCUSSION

Degenerative RCT is closely linked with chronic cuff tissue degeneration. Inflamm-aging (a chronic, sterile, low-grade inflammation state) is one of the most probable causes of chronic degenerative diseases.[15,16] Inflamm-aging leads to proinflammatory enzyme secretion, which negatively affects tissue homeostasis and, thus, adversely impacts tissue resident cells. Of all the impaired resident cells in degenerative cuff tendons, the senescence of TSPCs causes arguably the most detrimental effects of inflamm-aging, such as self-renewal defects and decreased differentiation potential to regenerate tenocytes.[17–19] In this study, we revealed that senescent TSPCs accumulate in degenerative rotator cuff tendons, which may serve as a potential therapeutic target for treating degenerative RCT.[20,21] Several studies have reported that the intrinsic pathogenic mechanisms of tendon degeneration can be traced back to TSPC senescence and dysfunction[6,11,22,23]; however, the intrinsic mechanisms underlying TSPC senescence are still unknown. Thus, further exploration of the mechanisms underlying inflamm-aging-induced TSPC senescence is an important first step for designing novel regenerative therapies.

During the aging process, the host defenses concurrently activate the inflammatory network and induce the release of SASP, including many proinflammatory factors.[24] The inflammatory network is largely related to the NF-κB pathway.[25] Meanwhile, recent clinical evidence has revealed that the NF-κB pathway plays a central role in RCT progression and therapy.[26–28] Hence, we hypothesized that NF-κB may serve as an intermediary of inflamm-aging-induced TSPC senescence. Increased NF-κBp-p65 expression and nuclear NF-κB p65 activation in S-TSPCs demonstrated NF-κB pathway activation in degenerative RCT. To further explore whether inhibiting the NF-κB pathway can improve inflamm-aging-induced TSPC senescence, the NF-κB pathway was blocked using siRNA transfection.

Figure 2. NF-κB signaling is activated during RCT development

(A) Western blotting for NF-κBp-p65 and NF-κBp65 and (B) quantification conforming the significantly increased NF-κB activation in S-TSPCs than that in H-TSPCs (n = 3 per group). (C) Immunofluorescence (green) staining and (D) quantification for NF-κBp65 revealing significantly increased nuclear NF-κBp65 localization in S-TSPCs than that in H-TSPCs. The red triangle indicates nuclear localization of NF-κBp65 (n = 3 per group). (E) Western blotting for NF-κBp-p65 and NF-κBp65 and (F) quantification conforming that IKKβ siRNA can significantly decrease NF-κB activation in IL-1β-induced senescent TSPCs (n = 3 per group). (G) Immunofluorescence (green) and (H) quantification for NF-κBp65 revealing that IKKβ siRNA can significantly decrease IL-1β-induced nuclear NF-κBp65 localization. The red triangle indicates nuclear localization of NF-κBp65 (n = 3 per group). (I) SA-β-gal staining and (J) quantification of senescent human TSPCs (n = 3 per group). (K) Immunofluorescence staining and (L) quantification of $p16^{INK4A}$ (red) and $p21^{CIP1}$ (green) (n = 3 per group). NF-κBp-p65, phosphorylated NF-κB p65. NF-κBp65, unphosphorylated NF-κB p65. *p < 0.05, **p < 0.01, ***p < 0.001.

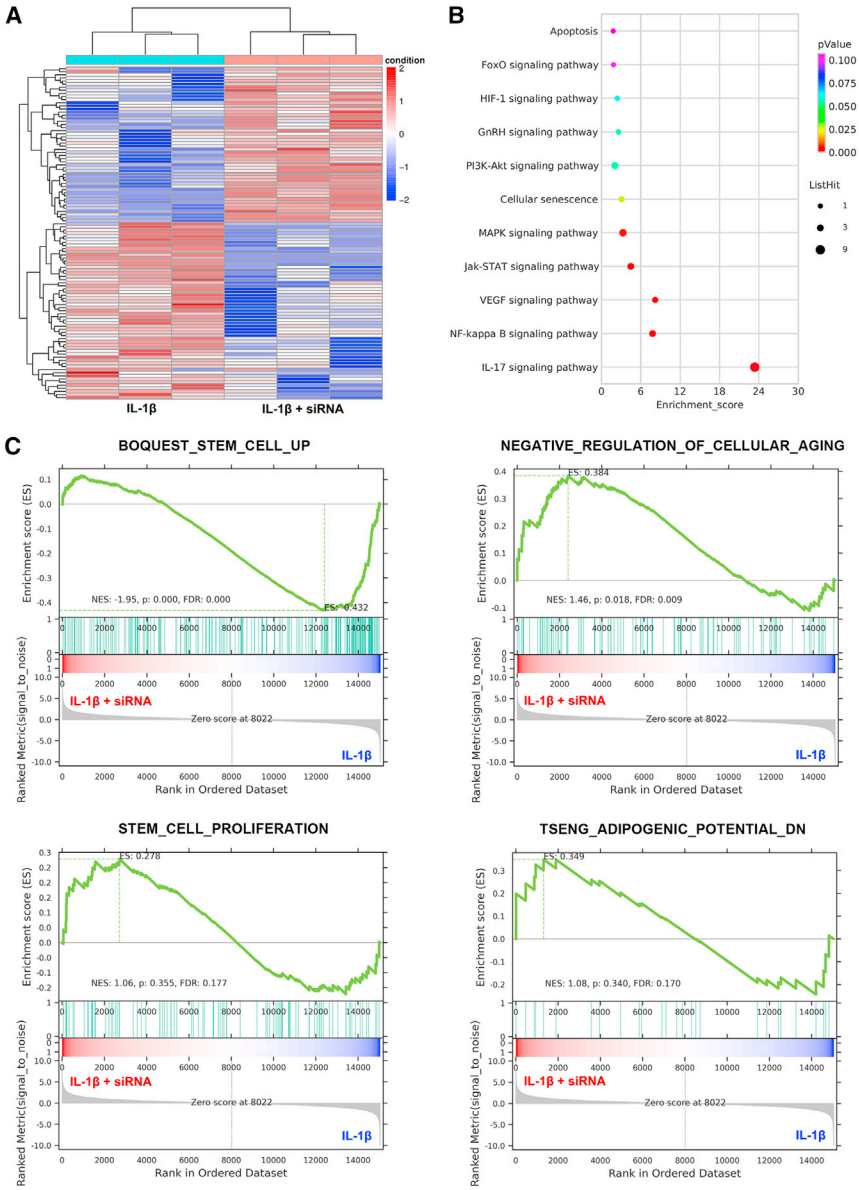

Figure 3. Blocking IKKβ mitigates TSPC senescence

(A) Heatmap representing the differential expression of 108 genes in IL-1β- and IL-1β + IKKβ siRNA-treated TSPCs. (B) Representative 10 downregulated pathways in IL-1β + IKKβ siRNA-treated TSPCs analyzed using the KEGG pathway. (C) Gene set enrichment analysis plots demonstrate that IL-1β- and IL-1β + IKKβ siRNA-treated TSPCs positively correlate with gene sets for stemness (BOQUEST STEM CELL UP), decreased cellular senescence (NEGATIVE REGULATION OF CELLULAR AGING), proliferation (STEM CELL PROLIFERATION), and decreased adipogenic potential (TSENG ADIPOGENIC POTENTIAL DN).

However, directly targeting the NF-κB protein complex (RelA/p65, RelB, c-Rel, p50/p105, and p52/p100) may alter its other essential biological functions.[29,30] IKKβ, one of the two homologous catalytic subunits essential for NF-κB activation, may serve as a target for inhibiting the release of NF-κB dimers from cytoplasmic inhibition and thus preventing NF-κB pathway activation.[30] Hence, four different siRNAs were designed and assayed for checking the highest IKKβ silencing efficiency in this study.

SiRNA is a class of double-stranded, non-coding RNA molecules that specifically interfere with gene expression by degrading mRNA and inhibiting targeted protein translation.[31] Unfortunately, rapid *in vivo* naked siRNA degradation and low penetration efficiency across cellular membranes currently restrict its clinical application.[32,33] RNase activity in human synovial fluid is similar to that in the serum, which is to catalyze naked siRNA degradation.[34] Therefore, an efficient delivery system that facilitates endocytosis and siRNA accumulation to interfere with specific genes *in vivo* is needed.[35,36] Numerous materials, such as viruses, cationic liposomes, inorganic nanoparticles, and polymers, have been developed to improve siRNA delivery.[36,37] Lately, AuNCs with excellent biocompatibility, low/non-cytotoxicity, and good stability have drawn increased attention to their potential for gene delivery.[38–40] Hence, self-assembled AuNC-siRNA was fabricated to achieve effective and convenient intra-articular IKKβ/NF-κB pathway silencing. To the best of our knowledge, AuNCs have not been used for intra-articular gene delivery previously. During the course of this study, AuNC-delivered siRNA was adopted to treat patients with recurrent glioblastoma in a first-in-human phase 0 clinical study, which further demonstrates the clinical translational potential of gold-based siRNA delivery in the human body.[41]

After blocking the NF-κB pathway, the unbiased sequencing approach and hierarchical clustering analysis revealed that NF-κB pathway suppression reversed the TSPC senescent phenotype. Cellular signaling mechanisms show that chronic inflammation stimulates p38MAPK signaling, thus inducing NF-κB pathway activation with a cellular senescence response.[42,43] Hence, NF-κB pathway blocking could be used as a target to downregulate inflamm-aging. To target block the NF-kB signaling pathway in tendon disease, IKKβ has been genetically deleted in mice tendon fibroblasts.[12] Conditional IKKβ knockout partially protected patients from overuse-induced tendinopathy, such as that caused by treadmill overuse. Additionally, both genetic deletion and pharmacological inhibition of IKKβ enhanced the tendon-to-bone repair of acute supraspinatus tendon tears.[12,44] While these studies reveal the potential role of

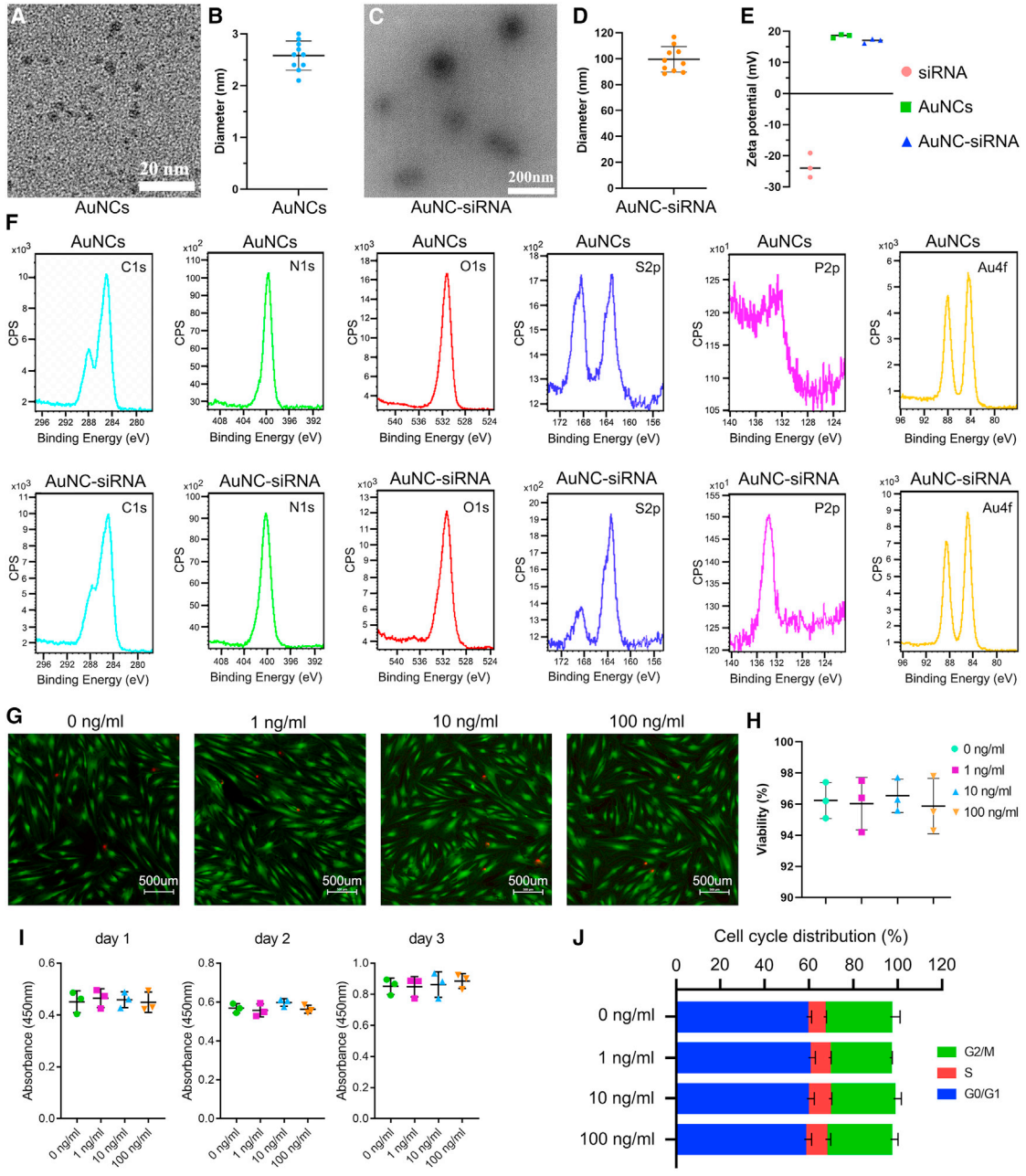

Figure 4. Preparation and characterization of AuNCs and AuNC-siRNA

(A) TEM images of AuNCs. (B) The mean diameter of AuNCs (n = 10 per group). (C) TEM images of AuNC-siRNA. (D) Mean diameter of AuNC-siRNA (n = 10 per group). (E) Surface charge of IKKβ siRNA, AuNCs, and AuNC-siRNA (n = 3 per group). (F) XPS for the C, N, O, S, P, and Au on AuNC and AuNC-siRNA surface. (G) Live/dead cell staining for TSPCs treated with different concentrations of AuNCs. Green fluorescence indicates live cells and red fluorescence indicates dead cells. (H) Quantification of TSPCs viability (n = 3 per group). (I) A Cell Counting Kit-8 assay for the effects of different AuNC concentrations on TSPCs proliferation (n = 3 per group). (J) The effects of different AuNCs concentrations on cell cycle distribution (n = 3 per group).

the IKKβ/NF-kB pathway in tendon disorders, relatively young animals and those with non-spontaneous degeneration-induced tendinopathy or tears only represent a small fraction of the rotator cuff disease cases seen clinically. Previous studies have revealed that advanced age impairs rotator cuff tendon-to-bone repair[45] and contributes to high-repetition, low-force, handle-pulling over-use-induced inflammation in supraspinatus tendons[46]; however, the underlying cellular mechanism is still vague. In this study,

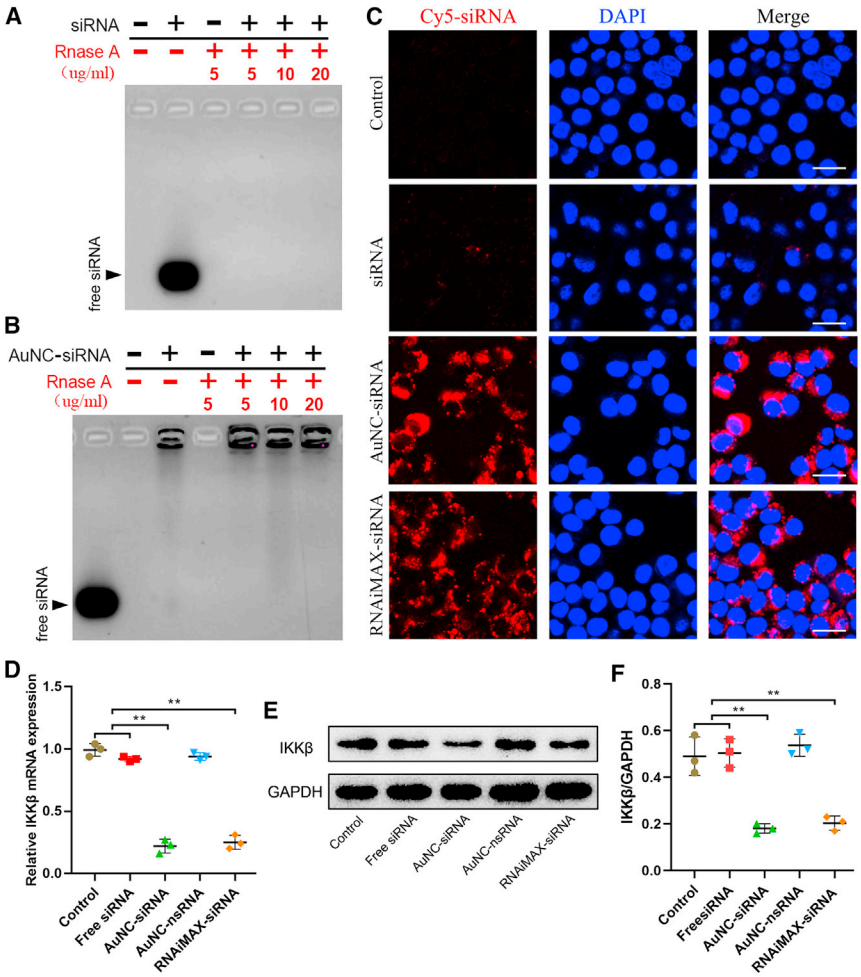

Figure 5. SiRNA protection and delivery efficiency of AuNC-siRNA

(A) Free siRNA degradation by RNase. (B) SiRNA protection in AuNC-siRNA against RNase. (C) Free siRNA and AuNC-siRNA uptake in TSPCs. SiRNA was labeled with Cy5 dye (Cy5–siRNA). Scale bars, 20 μm. (D) qRT-PCR assay of IKKβ mRNA expression (n = 3 per group). (E) Western blotting assay of the levels of IKKβ protein. (F) Relative IKKβ protein quantification in TSPCs normalized to GAPDH expression (n = 3 per group). **p < 0.01.

old rats (18 months old) with spontaneous inflamm-aging were used to understand the underlying intrinsic pathogenic mechanisms of degenerative RCT.[46,47] Although cellular senescence is generally seen as irreversible, the impact of inflamm-aging on skeletal stem and progenitor cells is thought to affect cell-extrinsic mechanisms instead of cell-intrinsic mechanisms inducing cellular senescence.[11,48,49] Hence, the detrimental effects of inflamm-aging on TSPC senescence are reversible by inhibiting IKKβ/NF-kB pathway, as demonstrated in this study.

Our study has certain limitations. First, we used healthy hamstring tendons as control samples. Clinically, the excision of healthy cuff tendons for research is not in line with ethical requirements and would not be approved by an ethics committee. Additionally, hamstring tendons are seldom affected by degenerative pathological changes, which can be demonstrated by the low percentage of senescent H-TSPCs. Second, the AuNC-assisted IKKβ siRNA delivery was not TSPC targeted. Thus, it may impair immune cell-mediated tendon repair. Hence, this therapeutic strategy should be optimized in future studies to target the TSPCs without impairing inflammation, which is necessary for tendon regeneration.[16]

All in all, this study demonstrates that the inflamm-aging-activated NF-kB pathway accounts for the underlying biological mechanism of TSPC senescence in degenerative RCT. The AuNC-assisted IKKβ siRNA delivery reduced inflamm-aging-triggered TSPC senescence by blocking the NF-kB pathway. Thus, intra-articular AuNC-siRNA administration may provide a novel therapeutic strategy for degenerative RCT.

MATERIALS AND METHODS

Study approval

This study was approved by the Ethics Committee of Shanghai Jiao Tong University Affiliated Sixth People's Hospital (Approval No: 2019-KY-047). Full informed consent was obtained from all patients before surgery. All animal studies were approved by the Institutional Animal Care and Use Committees of Shanghai Sixth People's Hospital.

Clinical samples

Degenerative supraspinatus tendons to be used as tendinopathy samples were taken from patients (n = 8; age 57–63 years; mean age, 60.9 ± 2.5 years) undergoing reverse shoulder arthroplasty surgery. The exclusion criteria are listed in Table S1.[50] Hamstring tendons were obtained from patients (n = 10; age 53–58 years; mean age, 54.8 ± 1.8 years) undergoing anterior cruciate ligament or posterior cruciate ligament reconstruction surgery to be used as healthy control samples.

Human TSPC isolation and culture

The tendon tissues were cut into small pieces and digested with 2 mg/mL collagenase type I (Sigma) for 2 h at 37°C. The digested tissue was washed using phosphate-buffered saline (PBS) and centrifuged at 1000 rpm for 5 min. The pelleted tissue was resuspended and cultured in α-MEM supplemented with 10% fetal bovine serum (FBS; Bibco) and 1% penicillin-streptomycin-neomycin at 37°C in a 5% CO_2

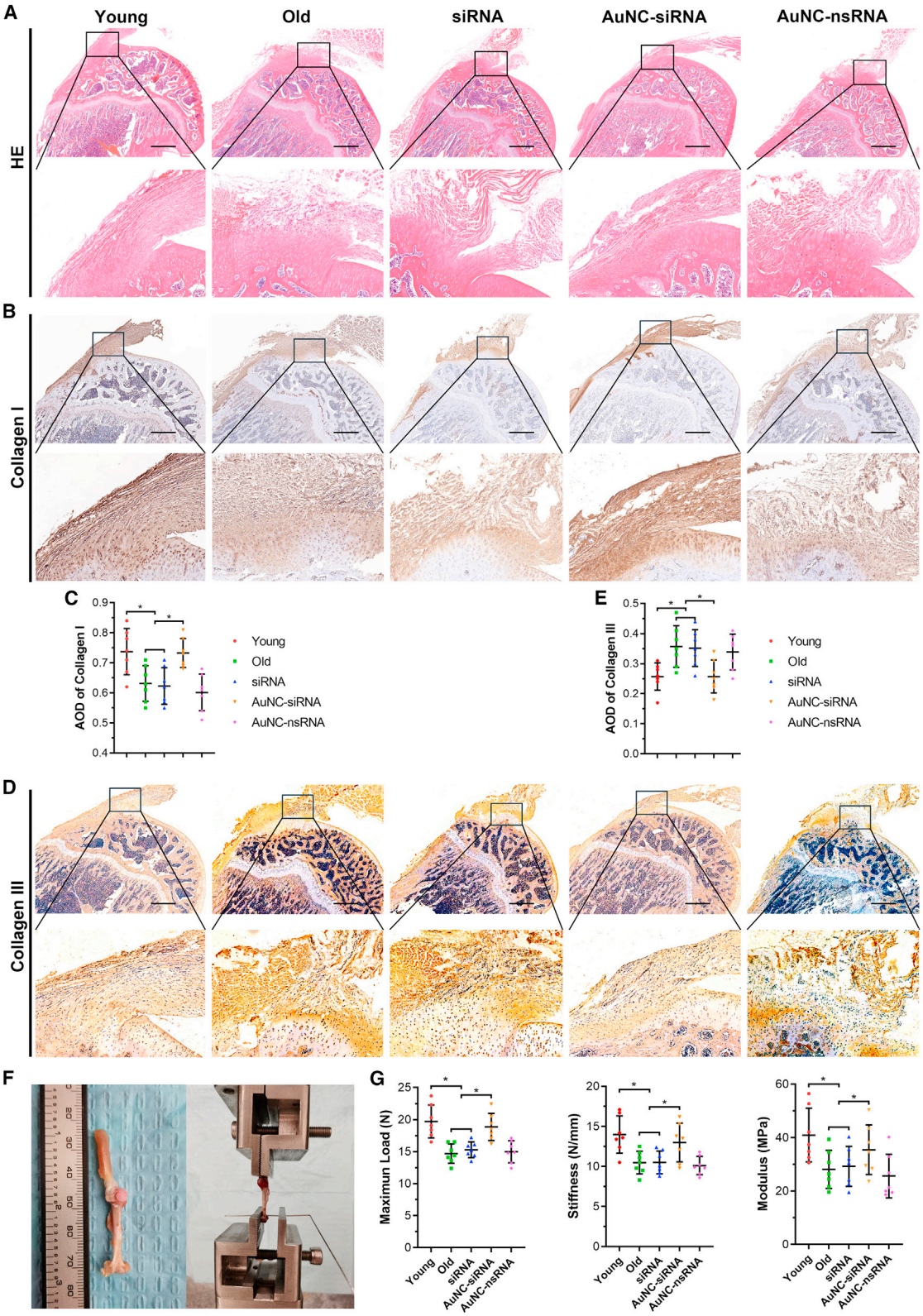

(legend on next page)

atmosphere. One-half of the culture medium was changed every 3 days. The tissues were removed on day 9. The passage-2 human TSPCs were used for *in vitro* study.[51]

TSPC identification

Flow cytometry analysis

TSPCs (5×10^5) were immunolabeled with 1 μg antigen-presenting cell (APC)- or PE-conjugated mouse human-specific antibodies for 1 h at 4°C. APC- or fluorescein isothiocyante-conjugated isotype-matched IgGs were used as controls. After washing three times with PBS containing 3% FBS, the stained TSPCs were subjected to fluorescence-activated cell sorting analysis (Beckman Coulter). The percentage of CD44, CD90, CD105, CD146, CD18, and CD34-positive cells was analyzed using FlowJo software. The details of antibodies used for flow cytometry analysis are listed in Table S5.

Multipotent differentiation

The TSPCs were induced for osteogenic, adipogenic, and chondrogenic differentiation analysis using previously established methods.[22] After induction, the cells were stained with Alizarin Red S (Servicebio) for osteogenesis analysis. The cell pellets, stained with Alcian blue (Servicebio) solution and type II collagen (1:400, Sigma, CP18) antibody, were used for chondrogenesis analysis. Oil Red O staining (Servicebio) was used for adipogenesis analysis. To quantify mineralization of Alizarin Red S staining, calcium deposits were incubated with 10% cetylpyridinium chloride (Sigma), and their concentration was measured at 570 nm absorbance. Quantification of the aggrecan-positive area and Oil Red O-positive area was performed using Image J software.

Senescent TSPC identification

Cell morphology

Phase-contrast images of primary S-TSPCs and H-TSPCs were captured to observe cell morphology. In addition to this, the S-TSPCs and H-TSPCs were stained with Phalloidin-iFluor488 (Abcam) and DAPI (Thermo) and imaged using a fluorescence microscope (Leica) to observe the actin cytoskeleton.

SA-β-gal staining

SA-β-gal staining was performed using an SA-β-gal staining kit (Beyotime Biotechnology) according to the methods used in several previous studies.[22,52,53] Briefly, the cells in 12-well plates were washed with PBS and fixed using 4% paraformaldehyde for 15 min. After washing three times with PBS, the SA-β-gal solution was added and incubated for 16 h at 37°C. Six random areas within each well were imaged to count 300 cells and calculate the percentage of SA-β-Gal-positive cells (blue in color).

Immunofluorescence

The S-TSPCs and H-TSPCs were routinely fixed with 4% paraformaldehyde (Servicebio), permeabilized with 0.5% Triton X-100 (Thermo), and blocked with 5% BSA (Beyotime). The cells were then incubated overnight with primary antibodies against $p16^{INK4A}$ (1:500, Abcam, ab54210) and $p21^{CIP1}$ (1:500, Abcam, ab109520) and incubated with Alexa Fluor 594- (1:1000, Abcam, ab150120) or Alexa Fluor 488-conjugated (1:1000, Abcam, ab150077) secondary antibodies.

Senescence marker mRNA level analysis

To analyze the expression of senescence-related genes, total RNA was extracted using TRIzol (Invitrogen) and reverse transcribed to cDNA using a TaqMan Reverse Transcription Kit. qRT-PCR assay was performed using the ABI7900 PCR system (Applied Biosystems) with SYBR green. The relative gene expression was calculated using the $2^{-\Delta\Delta Ct}$ method. The primer sequences are listed in Table S2.

Tenogenic potential

Tenogenic induction of H-TSPCs and S-TSPCs was performed as described in previous studies.[54,55] Briefly, H-TSPCs and S-TSPCs were seeded into 24-well plates with 90% confluence and cultured in low-glucose Dulbecco's modified Eagle's medium supplemented with 25 μM ascorbic acid (Sigma) and 25 ng/mL human connective tissue growth factor (PeproTech) to induce tenogenic differentiation. The medium was changed every 3 days. After 2 weeks, collagen deposition was visualized using Sirius red staining. Tenogenesis-related gene expression levels (*Scx*, *Bgn*, *Tnmd*, *Dcn*, *Col1*, and *Col3*) were assayed using qRT-PCR. The primer sequences are listed in Table S2.

NF-κB activation in senescent TSPCs

Western blotting analysis

To perform the Western blotting analysis, proteins were extracted from S-TSPCs and H-TSPCs using radioimmunoprecipitation assay buffer (Thermo) supplemented with protease inhibitors (Thermo) and phosphatase inhibitors (Thermo). After completing total protein quantification using the BCA Protein Assay Kit (Beyotime Biotechnology), equal amounts of total protein in each group were assayed and probed with antibodies against phospho-NF-κB p65 (1:1000, CST, 8242), NF-κB p65 (1:1000, CST, 3033), and GAPDH (1:1000, Abcam, ab8245). Horseradish peroxidase-linked anti-rabbit or anti-mouse IgG (Abcam) were used as a secondary antibody.

Immunofluorescence for p65 localization

To observe nuclear NF-κB p65 activation, the S-TSPCs and H-TSPCs were fixed in 4% paraformaldehyde for 10 min, washed three times with PBS, and permeabilized in 0.5% Triton X-100 (Thermo) for 15 min. After incubating with 5% BSA at room temperature for 1

Figure 6. Histological and biomechanical testing of supraspinatus–humerus complex

(A) H&E staining. (B) Immunohistochemical staining of type I collagen. (C) The average optimal density of type I collagen expressed in rat supraspinatus tendon (n = 7 per group). (D) Immunohistochemical staining of type III collagen. (E) The average optimal density of type III collagen expressed in rat supraspinatus tendon (n = 7 per group). (F) Images of the supraspinatus-humerus complex and biomechanical testing. (G) Tendon mechanical properties including maximum load, stiffness, and modulus (n = 7 per group). AOD, average optimal density. *$p < 0.05$.

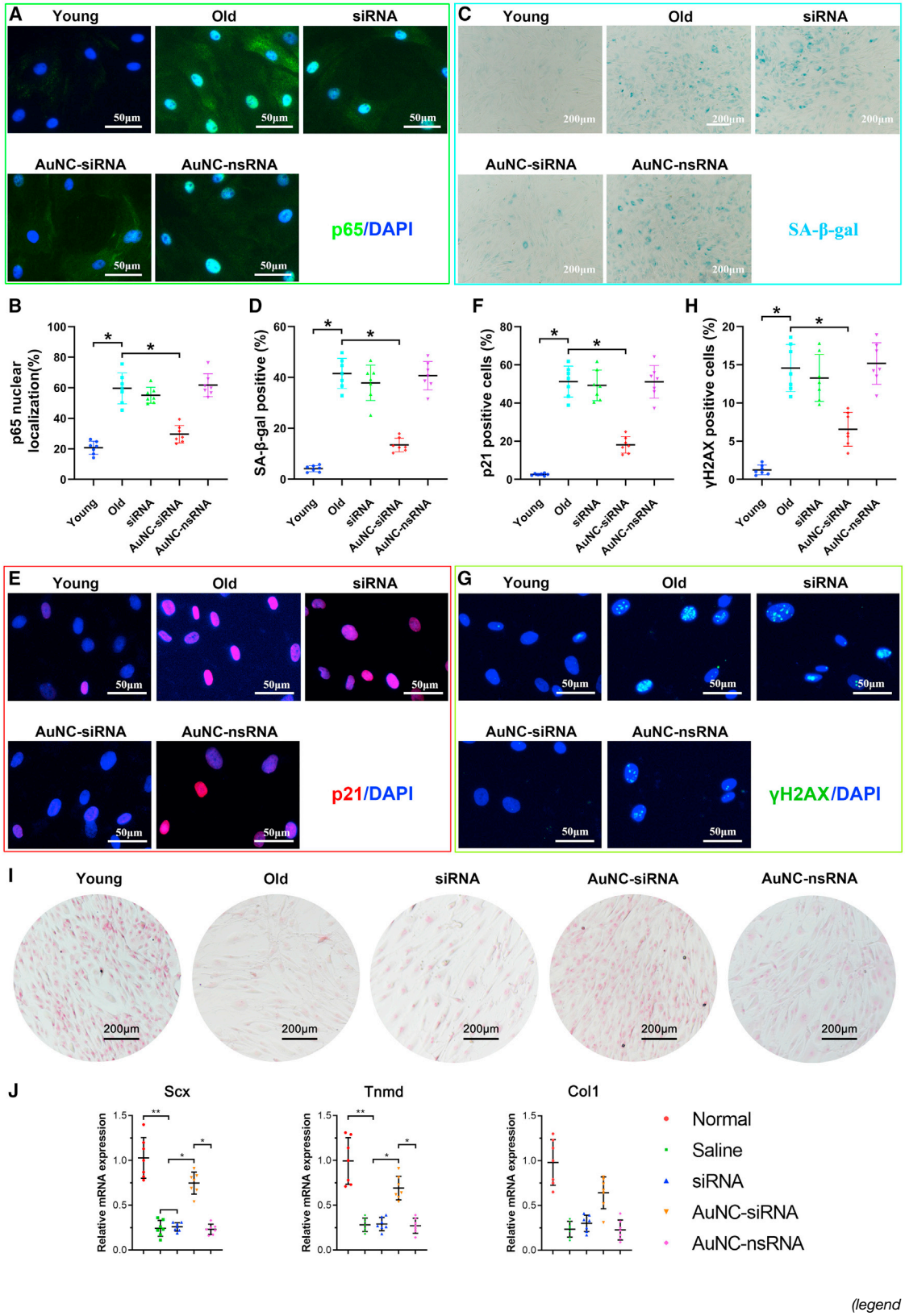

(legend on next page)

h, the cells were incubated overnight at 4°C with a primary antibody against NF-κB p65 (1:500), followed by a secondary antibody conjugated to Alexa Fluor 488 (1:200). The nuclei were labeled with DAPI (1:1000) for 5 min at room temperature. Images were captured using a fluorescence microscope (Leica Microsystems). Quantification of the percentage of positively stained cells was performed using the ImageJ software.

Screening effective IKKβ siRNA sequences

To determine the most effective IKKβ siRNA sequence, four different siRNA duplexes against human IKKβ and a nonsense siRNA (nsRNA) were purchased from GenePharma Biotechnology Company. The detailed siRNA sequences are listed in Table S3. For transfection, 60% confluent TSPCs in six-well plates were combined with 25 pmol siRNA duplex (each well) and 7.5 μL Lipofectamine RNAiMAX Reagent (Thermo). After transfecting for 48 h, IKKβ mRNA expression levels were assayed using qRT-PCR. The total proteins were extracted to analyze the IKKβ protein level using Western blotting. The siRNA that silenced the IKKβ/NF-κB pathway most effectively was selected for further studies.

Effect of IKKβ/NF-κB pathway blocking on TSPC senescence

H-TSPC senescence was induced *in vitro* using 10 ng/mL recombinant human IL-1β (PeproTech) for 24 h, as reported in a previous study.[56] To determine the effect of IKKβ blocking on preventing TSPC senescence, we pre-transfected TSPCs with IKKβ siRNA before incubating with IL-1β. After induction, nuclear NF-κB p65 activation, SA-β-Gal staining, and $p16^{INK4A}$ and $p21^{CIP1}$ immunofluorescence staining were assayed as mentioned above. Then, the RNA was sequenced (OE Biotechnology Company) to analyze the impact of IKKβ/NF-κB pathway blocking on TSPC senescence.

AuNC preparation, characterization, and biocompatibility

The AuNCs were synthesized through one-step reduction of Au^{3+}, oligoarginine peptide CRRRRRRRRR (CR_9, GL Biochem), and GSH (Sigma). Briefly, 100 mM $HAuCl_4$ (Sigma), 75 mM CR_9, and 150 mM GSH were blended in ultrapure water at 25°C. Then, the mixture was gently heated to 70°C and stirred at 500 rpm for 24 h. After fabrication, the size distribution and surface charge of the prepared nanomaterials were determined using dynamic light scattering (DLS; Malvern & Nano ZS). The morphology of the AuNCs was examined using a transmission electron microscope (TEM; Talos L120C G2).

To test the impact of AuNCs on TSPC proliferation, TSPCs (2×10^3 cells/well) were plated in 96-well plates and incubated with 0, 1, 10, or 100 nM AuNCs. After incubating for 24, 48, and 72 h, the number of viable TSPCs was measured using a Cell Counting Kit-8 (Dojindo) according to the manufacturer's instructions. To determine the *in vitro* cytotoxicity of AuNCs, TSPCs seeded into 24-well plates were incubated with 0, 1, 10, or 100 nM AuNCs for 24 h and stained using a Live/Dead Cell Double Staining Kit (Sigma). To analyze the effect of AuNCs on the cell cycle, TSPCs incubated with 0, 1, 10, or 100 nM AuNCs were stained using a DNA Content Quantitation Assay Kit (Solarbio) and assayed using flow cytometry (Beckman Coulter).

AuNC-siRNA complex fabrication, characterization, and stability

The anionic IKKβ siRNA (3 μg/mL) was mixed with cationic AuNCs (1 μg/mL) in ultrapure water and shaken on a benchtop incubator shaker (Eppendorf) for 1 h. After shaking, the self-assembled AuNC-siRNA was fabricated through electrostatic interaction. The nsRNA absorbed AuNCs (AuNC-nsRNA) were used as control.

The AuNC-siRNA surface charge was assayed using DLS. After this, the AuNC-siRNA morphology was examined by TEM. To detect its elemental composition, the samples were assayed using XPS. The stability of the AuNC-siRNA was evaluated using an RNase degradation assay. Briefly, the free siRNA and AuNC-siRNA were treated with 5, 10, or 20 μg/mL RNase for 10 min, and then RNase inhibitor was added to quench the enzymatic activity. The free siRNA and AuNC-siRNA were further run on a 20% (w/v) polyacrylamide gel at 160 V for 45 min, which was then stained using GelRed and imaged on a Gel Doc imaging system (Bio-Rad).

In vitro siRNA delivery and gene silencing efficiency of AuNC-siRNA

To observe the *in vitro* cellular uptake of siRNA, IKKβ siRNA was labeled with far-red fluorescent dye Cy5 (Cy5–siRNA, GenePharma Biotechnology Company). TSPCs (1×10^5 cells/well) were seeded in a 20-mm confocal dish (Nest) and incubated with 25 pmol free Cy5-siRNA, AuNC-Cy5-siRNA (Cy5-siRNA equivalent), or Cy5-siRNA with RNAiMAX Reagent. After incubating for 2 h, the medium was changed, the cells were washed three times with PBS, and cultured with fresh medium for another 48 h. Then, the total RNA and proteins were extracted to determine the levels of IKKβ mRNA and protein expression.

Animal experiments

Ten young (6 months old) and 40 old (18 months old) male Sprague-Dawley rats were used for *in vivo* studies. The 40 old rats were randomly assigned into four groups: old group (n = 10, non-treated), siRNA group (n = 10, siRNA treated), AuNC-siRNA group (n = 10, AuNC-siRNA treated), and AuNC-nsRNA group (n = 10, AuNC-nsRNA treated). The old rats were subacromially injected with

Figure 7. AuNC-siRNA retards rat TSPC senescence *in vivo*

(A and B) Immunofluorescence and quantification of NF-κBp65 in rat TSPCs isolated from different groups (n = 7 per group). (C and D) SA-β-gal staining of rat TSPCs isolated from different groups (n = 7 per group). (E and F) Immunofluorescence and quantification of $p21^{CIP1}$ in rat TSPCs isolated from different groups (n = 7 per group). (G and H) Immunofluorescence and quantification of γH2AX in rat TSPCs isolated from different groups (n = 7 per group). (I) Sirius red staining of tenogenic induced rat TSPCs (n = 7 per group). (J) qRT-PCR analysis of tenogenesis-related gene expression. *$p < 0.05$.

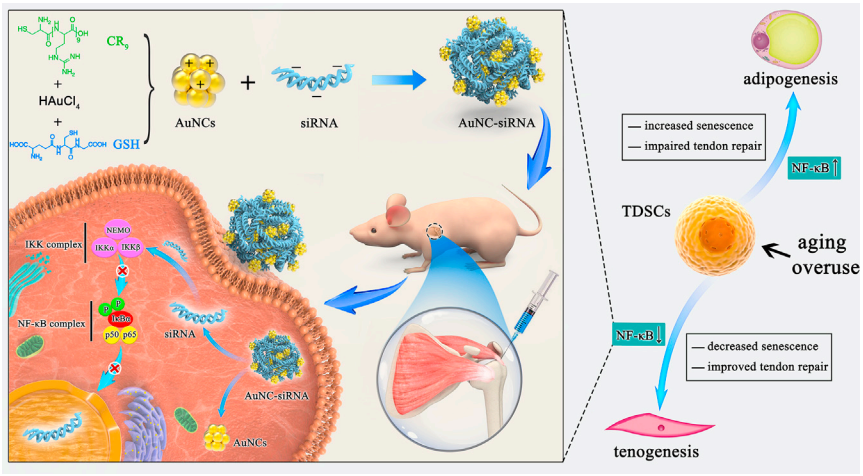

Figure 8. Schematic diagram of AuNC-siRNA for intra-articular NF-κB silencing to treat inflamm-aging triggered RCT by retarding TSPC senescence

1.5 nmol/20 μL siRNAs after identifying the posterolateral corner of the acromion with a 25G needle using methods reported in a previous study.[57] Three injections were administered at a intervals, according to methods established through previous studies.[58,59] One month after the third injection, the rats were euthanized to isolate the supraspinatus-humerus samples.

Ex vivo assay of rat TSPC senescence

The rat supraspinatus tendons were separated to isolate TSPCs with the method of human TSPC isolation described above. Passage-2 rat TSPCs were used for *ex vivo* assay of cellular senescence. Immunofluorescence staining and quantification of NF-κBp65 were performed to determine the *in vivo* efficiency of AuNC-siRNA on blocking IKKβ/NF-κB signaling. SA-β-gal staining and immunofluorescence staining of $p21^{CIP1}$ and γH2AX were performed and quantified to assay the *in vivo* effects of AuNC-siRNA on improving inflamm-aging-triggered TSPC senescence.

Ex vivo assay of rat TSPC tenogenic potential

Tenogenic induction of rat TSPCs was performed as described above. After induction for 2 weeks, collagen deposition was visualized using Sirius red staining. The expression of genes (*Scx*, *Tnmd*, *Col1*) associated with tenogenic differentiation was assayed using qRT-PCR. The primer sequences used are listed in Table S4.

Histological analysis

The samples used for histological analysis were routinely fixed in 10% neutral buffered formalin, decalcified with 10% EDTA, embedded in paraffin, and cut into 4 μm-thick sections.

To obtain an overview of the supraspinatus tendon, the sections were stained with H&E. To detect the specific expression levels of type I collagen and type III collagen, the sections were stained with collagen I antibody (1:500, Abcam, ab270993) and collagen III antibody (1:400, Abcam, ab6310).

Biomechanical testing

Before testing, the width and thickness of supraspinatus tendon insertion site on the greater tubercle were measured using a digital caliper to calculate the cross-sectional area. The specimens were fixed at a 0° abduction angle using a custom-designed material testing system (Instron Corp.) as described in a previous study.[60,61] Briefly, the humerus was secured using a 0.8-mm Kirschner wire, and the supraspinatus belly was secured using a screw grip. The specimen was preloaded with 0.1 N and loaded to failure at the rate of 10 mm/min. The ultimate load-to-failure and load-displacement curves were recorded to calculate the stiffness and modulus.

Statistical analysis

All data are shown as mean ± standard deviation. One-way analysis of variance with the *post hoc* Tukey test or Student *t* test was used to analyze the statistical differences between different groups using GraphPad Prism 8 software. A p value of less than 0.05 was considered statistically significant.

SUPPLEMENTAL INFORMATION

Supplemental information can be found online at https://doi.org/10.1016/j.omtn.2021.12.026.

ACKNOWLEDGMENTS

This research was funded by the National Natural Science Foundation of China (82072401, 81871755), the Program of Shanghai Academic/Technology Research Leader (19XD1402800), the Shanghai Municipal Education Commission Scientific Research and Innovation Program (2021-01-07-00-02-E00082), the Clinical Research Center of Shanghai University of Medicine & Health Sciences (20MC2020003), the Academician Expert Workstation of the Jinshan District (jszjz2020007Y), and the Plan of Medical Key Specialty Construction, and the Shanghai Health Committee (ZK2019B03).

AUTHOR CONTRIBUTIONS

Conceptualization, C.W., D.C., F.X., and Y.H.; Methodology, C.W., Z.Z., W.S., Z.C., and Z. D; Investigation, C.W., Z.Z., F.X., W.S., and Z.C.; Visualization, C.W., Z.Z., W.S., and Z.C.; Funding acquisition, Y.H.; Project administration, Y.H.; Supervision: Y.H.; Writing - original draft, C.W., Z.Z.; Writing - review & editing: C.W., F.X., and Y.H. All authors read and approved the final version of the manuscript.

DECLARATION OF INTERESTS

The authors declare no competing interests.

REFERENCES

1. Urwin, M., Symmons, D., Allison, T., Brammah, T., Busby, H., Roxby, M., Simmons, A., and Williams, G. (1998). Estimating the burden of musculoskeletal disorders in the community: the comparative prevalence of symptoms at different anatomical sites, and the relation to social deprivation. Ann. Rheum. Dis. *57*, 649–655.
2. Cederqvist, S., Flinkkilä, T., Sormaala, M., Ylinen, J., Kautiainen, H., Irmola, T., Lehtokangas, H., Liukkonen, J., Pamilo, K., Ridanpää, T., et al. (2020). Non-surgical and surgical treatments for rotator cuff disease: a pragmatic randomised clinical trial with 2-year follow-up after initial rehabilitation. Ann. Rheum. Dis. *80*, 796–802.
3. Li, L., Bokshan, S.L., Ready, L.V., and Owens, B.D. (2019). The primary cost drivers of arthroscopic rotator cuff repair surgery: a cost-minimization analysis of 40,618 cases. J. Shoulder Elbow Surg. *28*, 1977–1982.
4. Selim, N.M., and Badawy, E.R. (2021). Consider long head of biceps tendon for reconstruction of massive, irreparable rotator cuff tear. Arthrosc. Tech. *10*, e457–e467.
5. Dang, A., and Davies, M. (2018). Rotator cuff disease: treatment options and considerations. Sports Med. Arthrosc. Rev. *26*, 129–133.
6. Nicaise, A.M., Wagstaff, L.J., Willis, C.M., Paisie, C., Chandok, H., Robson, P., Fossati, V., Williams, A., and Crocker, S.J. (2019). Cellular senescence in progenitor cells contributes to diminished remyelination potential in progressive multiple sclerosis. Proc. Natl. Acad. Sci. U S A *116*, 9030–9039.
7. Childs, B.G., Durik, M., Baker, D.J., and van Deursen, J.M. (2015). Cellular senescence in aging and age-related disease: from mechanisms to therapy. Nat. Med. *21*, 1424–1435.
8. Chung, H.Y., Kim, D.H., Lee, E.K., Chung, K.W., Chung, S., Lee, B., Seo, A.Y., Chung, J.H., Jung, Y.S., Im, E., et al. (2019). Redefining chronic inflammation in aging and age-related diseases: proposal of the senoinflammation concept. Aging Dis. *10*, 367–382.
9. Franceschi, C., Garagnani, P., Parini, P., Giuliani, C., and Santoro, A. (2018). Inflammaging: a new immune-metabolic viewpoint for age-related diseases. Nat. Rev. Endocrinol. *14*, 576–590.
10. Oh, J., Lee, Y.D., and Wagers, A.J. (2014). Stem cell aging: mechanisms, regulators and therapeutic opportunities. Nat. Med. *20*, 870–880.
11. Josephson, A.M., Bradaschia-Correa, V., Lee, S., Leclerc, K., Patel, K.S., Muinos Lopez, E., Litwa, H.P., Neibart, S.S., Kadiyala, M., Wong, M.Z., et al. (2019). Age-related inflammation triggers skeletal stem/progenitor cell dysfunction. Proc. Natl. Acad. Sci. U S A *116*, 6995–7004.
12. Abraham, A.C., Shah, S.A., Golman, M., Song, L., Li, X., Kurtaliaj, I., Akbar, M., Millar, N.L., Abu-Amer, Y., Galatz, L.M., and Thomopoulos, S. (2019). Targeting the NF-κB signaling pathway in chronic tendon disease. Sci. Transl. Med. *11*, eaav4319.
13. Han, S.H., Kim, H.K., Ahn, J.H., Lee, D.H., Baek, M., Ye, G., Lee, J.M., Min, K., Oh, C., and Lee, S. (2018). A protocol to acquire the degenerative tenocyte from humans. J. Vis. Exp. *9*, 57634.
14. Jo, C.H., Kim, J.E., Yoon, K.S., and Shin, S. (2012). Platelet-rich plasma stimulates cell proliferation and enhances matrix gene expression and synthesis in tenocytes from human rotator cuff tendons with degenerative tears. Am. J. Sports Med. *40*, 1035–1045.
15. Franceschi, C., Bonafè, M., Valensin, S., Olivieri, F., De Luca, M., Ottaviani, E., and De Benedictis, G. (2000). Inflamm-aging. An evolutionary perspective on immunosenescence. Ann. N. Y. Acad. Sci. *908*, 244–254.
16. Bernard, N.J. (2019). Bone inflamm-ageing. Nat. Rev. Rheumatol. *15*, 252.
17. Pawlikowski, B., Betta, N.D., Antwine, T., and Olwin, B.B. (2019). Skeletal muscle stem cell self-renewal and differentiation kinetics revealed by EdU lineage tracing during regeneration. bioRxiv, 627851. https://doi.org/10.1101/627851.
18. Pajarinen, J., Lin, T., Gibon, E., Kohno, Y., Maruyama, M., Nathan, K., Lu, L., Yao, Z., and Goodman, S.B. (2019). Mesenchymal stem cell-macrophage crosstalk and bone healing. Biomaterials *196*, 80–89.
19. van Velthoven, C.T.J., and Rando, T.A. (2019). Stem cell quiescence: dynamism, restraint, and cellular Idling. Cell Stem Cell *24*, 213–225.
20. Jeon, O.H., Kim, C., Laberge, R.M., Demaria, M., Rathod, S., Vasserot, A.P., Chung, J.W., Kim, D.H., Poon, Y., David, N., et al. (2017). Local clearance of senescent cells attenuates the development of post-traumatic osteoarthritis and creates a pro-regenerative environment. Nat. Med. *23*, 775–781.
21. Johmura, Y., Yamanaka, T., Omori, S., Wang, T.-W., Sugiura, Y., Matsumoto, M., Suzuki, N., Kumamoto, S., Yamaguchi, K., Hatakeyama, S., et al. (2021). Senolysis by glutaminolysis inhibition ameliorates various age-associated disorders. Science *371*, 265–270.
22. Kohler, J., Popov, C., Klotz, B., Alberton, P., Prall, W.C., Haasters, F., Muller-Deubert, S., Ebert, R., Klein-Hitpass, L., Jakob, F., et al. (2013). Uncovering the cellular and molecular changes in tendon stem/progenitor cells attributed to tendon aging and degeneration. Aging Cell *12*, 988–999.
23. Zhou, Z., Akinbiyi, T., Xu, L., Ramcharan, M., Leong, D.J., Ros, S.J., Colvin, A.C., Schaffler, M.B., Majeska, R.J., Flatow, E.L., and Sun, H.B. (2010). Tendon-derived stem/progenitor cell aging: defective self-renewal and altered fate. Aging Cell *9*, 911–915.
24. Salminen, A., and Kaarniranta, K. (2010). Genetics vs. entropy: longevity factors suppress the NF-kappaB-driven entropic aging process. Ageing Res. Rev. *9*, 298–314.
25. Gilmore, T.D., and Wolenski, F.S. (2012). NF-κB: where did it come from and why? Immunol. Rev. *246*, 14–35.
26. Tang, C., Chen, Y., Huang, J., Zhao, K., Chen, X., Yin, Z., Heng, B.C., Chen, W., and Shen, W. (2018). The roles of inflammatory mediators and immunocytes in tendinopathy. J. Orthop. Translat. *14*, 23–33.
27. Abraham, A.C., Shah, S.A., and Thomopoulos, S. (2017). Targeting inflammation in rotator cuff tendon degeneration and repair. Tech. Shoulder Elb. Surg. *18*, 84–90.
28. Abraham, A.C., Shah, S.A., Golman, M., Song, L., Li, X., Kurtaliaj, I., Akbar, M., Millar, N.L., Abu-Amer, Y., Galatz, L.M., and Thomopoulos, S. (2019). Targeting the NF-κB signaling pathway in chronic tendon disease. Sci. Transl. Med. *11*, eaav4319.
29. Kondylis, V., Kumari, S., Vlantis, K., and Pasparakis, M. (2017). The interplay of IKK, NF-κB and RIPK1 signaling in the regulation of cell death, tissue homeostasis and inflammation. Immunol. Rev. *277*, 113–127.
30. Yu, H., Lin, L., Zhang, Z., Zhang, H., and Hu, H. (2020). Targeting NF-κB pathway for the therapy of diseases: mechanism and clinical study. Signal. Transduct. Target. Ther. *5*, 209.
31. Yu, A.M., Choi, Y.H., and Tu, M.J. (2020). RNA drugs and RNA targets for small molecules: principles, progress, and challenges. Pharmacol. Rev. *72*, 862–898.
32. Mandal, A., Kumbhojkar, N., Reilly, C., Dharamdasani, V., Ukidve, A., Ingber, D.E., and Mitragotri, S. (2020). Treatment of psoriasis with NFKBIZ siRNA using topical ionic liquid formulations. Sci. Adv. *6*, eabb6049.
33. Dong, Y., Siegwart, D.J., and Anderson, D.G. (2019). Strategies, design, and chemistry in siRNA delivery systems. Adv. Drug Deliv. Rev. *144*, 133–147.
34. Elena, N., Rebecca, H., Uwe, L., and Ulf, M.-L. (2018). The role of extracellular nucleic acids in rheumatoid arthritis. Curr. Pharm. Biotechnol. *19*, 1182–1188.
35. Wen, Y., Bai, H., Zhu, J., Song, X., Tang, G., and Li, J. (2020). A supramolecular platform for controlling and optimizing molecular architectures of siRNA targeted delivery vehicles. Sci. Adv. *6*, eabc2148.
36. Grun, M.K., Suberi, A., Shin, K., Lee, T., Gomerdinger, V., Moscato, Z.M., Piotrowski-Daspit, A.S., and Saltzman, W.M. (2021). PEGylation of poly(amine-co-ester) polyplexes for tunable gene delivery. Biomaterials *272*, 120780.
37. Zhang, Z., Zhao, X., Wang, D., Moreira, D., Su, Y.-L., Alcantara, M., Swiderski, P., Wong, J., Hui, S., Forman, S., et al. (2021). Targeted in vivo delivery of NF-κB decoy inhibitor augments sensitivity of B cell lymphoma to therapy. Mol. Ther. *29*, 1214–1225.
38. Zhang, L., Wang, L., Xie, Y., Wang, P., Deng, S., Qin, A., Zhang, J., Yu, X., Zheng, W., and Jiang, X. (2019). Triple-targeting delivery of CRISPR/Cas9 to reduce the risk of cardiovascular diseases. Angew. Chem. Int. Ed. *58*, 12404–12408.
39. Wang, P., Zhang, L., Xie, Y., Wang, N., Tang, R., Zheng, W., and Jiang, X. (2017). Genome editing for cancer therapy: delivery of Cas9 protein/sgRNA plasmid via a gold nanocluster/lipid core–shell nanocarrier. Adv. Sci. *4*, 1700175.
40. Lei, Y., Tang, L., Xie, Y., Xianyu, Y., Zhang, L., Wang, P., Hamada, Y., Jiang, K., Zheng, W., and Jiang, X. (2017). Gold nanoclusters-assisted delivery of NGF siRNA for effective treatment of pancreatic cancer. Nat. Commun. *8*, 15130.

41. Kumthekar, P., Ko, C.H., Paunesku, T., Dixit, K., Sonabend, A.M., Bloch, O., Tate, M., Schwartz, M., Zuckerman, L., Lezon, R., et al. (2021). A first-in-human phase 0 clinical study of RNA interference–based spherical nucleic acids in patients with recurrent glioblastoma. Sci. Transl. Med. *13*, eabb3945.

42. Salminen, A., Kauppinen, A., and Kaarniranta, K. (2012). Emerging role of NF-κB signaling in the induction of senescence-associated secretory phenotype (SASP). Cell. Signal. *24*, 835–845.

43. Freund, A., Patil, C.K., and Campisi, J. (2011). p38MAPK is a novel DNA damage response-independent regulator of the senescence-associated secretory phenotype. EMBO. J. *30*, 1536–1548.

44. Golman, M., Li, X., Skouteris, D., Abraham, A.A., Song, L., Abu-Amer, Y., and Thomopoulos, S. (2021). Enhanced tendon-to-bone healing via IKKβ inhibition in a rat rotator cuff model. Am. J. Sports Med. *49*, 780–789.

45. Plate, J.F., Brown, P.J., Walters, J., Clark, J.A., Smith, T.L., Freehill, M.T., Tuohy, C.J., Stitzel, J.D., and Mannava, S. (2014). Advanced age diminishes tendon-to-bone healing in a rat model of rotator cuff repair. Am. J. Sports Med. *42*, 859–868.

46. Kietrys, D.M., Barr-Gillespie, A.E., Amin, M., Wade, C.K., Popoff, S.N., and Barbe, M.F. (2012). Aging contributes to inflammation in upper extremity tendons and declines in forelimb agility in a rat model of upper extremity overuse. PLoS One *7*, e46954.

47. Swan, M.A., Sato, E., Galatz, L.M., Thomopoulos, S., and Ward, S.R. (2014). The effect of age on rat rotator cuff muscle architecture. The effect of age on rat rotator cuff muscle architecture. J. Shoulder Elbow Surg. *23*, 1786–1791.

48. Kovtonyuk, L.V., Fritsch, K., Feng, X., Manz, M.G., and Takizawa, H. (2016). Inflamm-aging of hematopoiesis, hematopoietic stem cells, and the bone marrow microenvironment. Front. Immunol. *7*, 502.

49. Lee, B.-C., and Yu, K.-R. (2020). Impact of mesenchymal stem cell senescence on Inflammaging. BMB Rep. *53*, 65–73.

50. Plate, J.F., Pace, L.A., Seyler, T.M., Moreno, R.J., Smith, T.L., Tuohy, C.J., and Mannava, S. (2014). Age-related changes affect rat rotator cuff muscle function. J. Shoulder Elbow Surg. *23*, 91–98.

51. Bi, Y., Ehirchiou, D., Kilts, T.M., Inkson, C.A., Embree, M.C., Sonoyama, W., Li, L., Leet, A.I., Seo, B.M., Zhang, L., et al. (2007). Identification of tendon stem/progenitor cells and the role of the extracellular matrix in their niche. Nat. Med. *13*, 1219–1227.

52. Han, W., Wang, B., Liu, J., and Chen, L. (2017). The p16/miR-217/EGR1 pathway modulates age-related tenogenic differentiation in tendon stem/progenitor cells. Acta Biochim. Biophys. Sin. *49*, 1015–1021.

53. Chen, M., Li, Y., Xiao, L., Dai, G., Lu, P., Wang, Y., and Rui, Y. (2020). AQP1 modulates tendon stem/progenitor cells senescence during tendon aging. Cell Death Dis. *11*, 193.

54. Lui, P.P.Y., Wong, O.T., and Lee, Y.W. (2016). Transplantation of tendon-derived stem cells pre-treated with connective tissue growth factor and ascorbic acid in vitro promoted better tendon repair in a patellar tendon window injury rat model. Cytotherapy *18*, 99–112.

55. Ni, M., Rui, Y.F., Tan, Q., Liu, Y., Xu, L.L., Chan, K.M., Wang, Y., and Li, G. (2013). Engineered scaffold-free tendon tissue produced by tendon-derived stem cells. Biomaterials *34*, 2024–2037.

56. Xu, K., Lin, C., Ma, D., Chen, M., Zhou, X., He, Y., Moqbel, S.A.A., Ma, C., and Wu, L. (2021). Spironolactone ameliorates senescence and calcification by modulating autophagy in rat tendon-derived stem cells via the NF-κB/MAPK pathway. Oxid. Med. Cell. Longev. *2021*, 5519587.

57. Maman, E., Yehuda, C., Pritsch, T., Morag, G., Brosh, T., Sharfman, Z., and Dolkart, O. (2016). Detrimental effect of repeated and single subacromial corticosteroid injections on the intact and injured rotator cuff: a biomechanical and imaging study in rats. Am. J. Sports Med. *44*, 177–182.

58. Huang, P.-H., Wang, C.-J., Chou, W.-Y., Wang, J.-W., and Ko, J.-Y. (2017). Short-term clinical results of intra-articular PRP injections for early osteoarthritis of the knee. Int. J. Surg. *42*, 117–122.

59. Concoff, A., Sancheti, P., Niazi, F., Shaw, P., and Rosen, J. (2017). The efficacy of multiple versus single hyaluronic acid injections: a systematic review and meta-analysis. BMC. Musculoskelet. Disord. *18*, 542.

60. Yonemitsu, R., Tokunaga, T., Shukunami, C., Ideo, K., Arimura, H., Karasugi, T., Nakamura, E., Ide, J., Hiraki, Y., and Mizuta, H. (2019). Fibroblast growth factor 2 enhances tendon-to-bone healing in a rat rotator cuff repair of chronic tears. Am. J. Sports Med. *47*, 1701–1712.

61. Newton, M.D., Davidson, A.A., Pomajzl, R., Seta, J., Kurdziel, M.D., and Maerz, T. (2016). The influence of testing angle on the biomechanical properties of the rat supraspinatus tendon. J. Biomech. *49*, 4159–4163.